Chemical stabilization of gold coated by silver core-shell nanoparticles *via* electron transfer

Cheshta Shankar, Anh T N Dao, Prerna Singh, Koichi Higashimine, Derrick M Mott and Shinya Maenosono
Japan Advanced Institute of Science and Technology, School of Materials Science, 1-1 Asahidai, Nomi, Ishikawa, 923-1292, Japan

E-mail: derrickm@jaist.ac.jp

Abstract. Silver nanoparticles are notoriously susceptible to oxidation, yet gold nanoparticles coated in silver exhibit a unique electronic interaction that occurs at the interface of the two metals, leading to enhanced stability properties for the silver shell. In order to probe the phenomenon, the stability of gold nanoparticles coated by silver was studied in the presence of various chloride containing electrolytes. It was found that a critical silver shell thickness of approximately 1 nm exists that cannot be oxidatively etched from the particle surface, this is in contrast to the observation of complete oxidative etching for monometallic silver nanoparticles. The results are discussed in terms of particle composition, structure, and morphology before and after exposing the particles to the electrolytes. Raman analysis of the reporter molecule 3-amino-1,2,4-triazole-5-thiol adsorbed to the particle surface illustrates the feasibility of using gold coated by silver nanoparticle probes in sensing applications that require the presence of high levels of salt. The results provide insight on the manipulation of the electronic and stability properties for gold and silver based nanoparticles.

Subject Classification Numbers (PACS): 73.63.Bd, 81.07.Bc, 61.46.Df

Submitted to: Nanotechnology

1. Introduction

Nanoparticles (NPs) have been intensively studied as a result of the new, unique and oftentimes unexpected properties displayed by nanoscale materials. As a result, NPs are beginning to find use in a wide range of practical applications including catalysis, thermoelectrics, microelectronics, sensing, and bio-diagnostics [1-4]. The area of bio-molecular sensing and diagnostics is perhaps one of the most significant technology areas to benefit from the unique properties of NPs because of the greatly increased level of bio-molecular detection

sensitivity that can be achieved when compared to traditional detection techniques [5]. As a result, nanotechnology has the potential to increase quality of care through earlier detection of diseases, easier detection of malady that is traditionally challenging to detect, and cheaper/more mobile detection methods, in addition to other advantages [5-7]. It is the unique optical/electronic properties of NPs that has been demonstrated to lead to the advances in bio-molecular sensing and diagnostics [5,6,8]. Some of the best examples of well-studied NP probes with enhanced optical/electronic properties include both gold (Au) and silver (Ag) which possess well defined localized surface plasmon resonance (LSPR) bands in the UV-Visible (UV-Vis) region of the electromagnetic spectrum [8,9]. This LSPR is the property that ultimately is utilized for the advanced bio-molecular detection, either through observing changes to the position of the LSPR band in UV-Vis before and after exposure to an analyte [7], or through enhanced Raman spectroscopy [10]. Au NPs have perhaps received the most attention as a bio-molecular probe because of the relatively high molar extinction coefficient and a very high resistance to oxidation [5,7]. Ag NPs have also received a significant amount of attention because it possesses the highest molar extinction coefficient for any metal [2,5,6]. However, monometallic Ag NPs have found limited practical use because of a severe susceptibility to oxidation, which oftentimes makes the sensing results for these particles non-reproducible [5]. As a result, many works have been attempted to combine Au and Ag into a single functional nanoprobe that has the very high molar extinction coefficient of Ag and the chemical stability of Au. The most popular solution has been to create a core@shell type of structure where Ag NPs are first synthesized, then Au is coated on the outside as a shell [5,6,8]. The expectation is that the Ag core will contribute a high molar extinction coefficient while the Au shell protects the core from oxidation. In practical terms, the Ag@Au structure has shown many drawbacks, including high suppression of the optical properties of Ag by the Au shell, as well as significant challenges in synthesizing a probe with uniform structure [6,8]. In most cases, the relatively high reduction potential of Au causes Ag to be oxidized in the coating process, leading to structures with hollow cores, non-continuous Au shell, or formation of alloys [8,11,12]. Such particles display non-controllable optical/electronic properties, and are inherently instable because of the exposure of Ag to the outside environment, making them non-ideal for sensing applications.

Despite the challenges, the Au/Ag NP system is still very attractive as a platform for bio-molecular sensing and diagnostics. The key to the successful implementation of these materials is the ability to create a stable and robust particle with controllable optical/electronic properties. One promising technique towards this goal is the use of

Au to modify the electronic properties of Ag to increase the stability against oxidation and/or galvanic etching [13]. This has recently been demonstrated by creating an inverse core@shell structure (i.e. Au@Ag), where Au is used as the core and Ag as the shell [14,15]. The Au core serves as a platform for regulating the overall particle size and also modifies the electronic characteristics of the deposited Ag shell [14]. The creation of such a structure has several advantages including increased particle dispersity [16], the LSPR features of the Ag are not suppressed by an outer Au shell, and the Ag shell becomes oxidation resistant [14]. It has been demonstrated that the Ag in this inverted Au@Ag structure shows both an enhanced resistance to oxidation and the galvanic replacement reaction by gold ions, allowing this type of particle to be coated in a second uniform Au shell (at the expense of some of the LSPR features of the Ag) [14]. In fact, the Au@Ag NP structure has received much attention in the literature [12,16-19], however, no previous studies have focused on controlling the thickness of the outer Ag shell to exist in a range that would exhibit the modified electronic properties, which is the key to harnessing the unique electronic interaction between Au and Ag to increase the resistance of Ag to oxidation [14]. The electronic interaction between Au and Ag is counterintuitive because Au is traditionally thought of as "highly electronegative" which implies that Au will in general withdraw electrons from Ag. However, realistically, the electronic interaction between Au and Ag is quite complicated, with Au gaining non-*d* orbital charge and losing *d* orbital charge while Ag gains *d* charge and loses non-*d* charge in an alloy system [13]. This charge re-distribution is essentially what causes the Ag to gain the enhanced stability properties in the Au@Ag NP system [14,15] It is also important to note that the enhanced stability of the Ag is distance dependent from the Au core. The farther the Ag is from the Au core (the thicker the Ag shell) the weaker the stability enhancement becomes. While the traditional Ag@Au structure (and alloys) also exhibits the electronic transfer phenomenon, the key to creating high optical activity and stable probes is the manipulation of the particle size, shape, structure and surface properties, which is hampered by the galvanic replacement reaction when Au is used to coat Ag NPs.

In order to clarify the parameters that affect the enhanced stability of Ag in the Au@Ag structure, the relative stability of these probes was tested when exposed to various electrolytes, including chloride containing salts and acid such as sodium chloride (NaCl), calcium chloride ($CaCl_2$) and hydrochloric acid (HCl). Addressing the stability of this class of NP probe in the presence of such electrolytes is essentially important, because the detection of many bio-molecules typically requires a buffer solution which contains significant amount of chloride containing electrolyte/salt including NaCl, KCl, $CaCl_2$, $MgCl_2$, and HCl [20], for example DNA will not

denature without the presence of biological levels of salt [5]. In addition, the exposure of Ag to the ambient atmosphere as well as chloride anions (Cl^-) is well known to lead to oxidative dissolution of the Ag, destroying Ag based particles [3,21,22]. The formation and ultimate understanding of how to manipulate the particle stability, optical, and electronic properties is expected to lead to more ready accessibility of highly active and robust NP probes for practical bio-molecular sensing and diagnostics applications.

2. Experimental

2.1. Chemicals

Gold tetrachloroaurate trihydrate ($HAuCl_4 \cdot 3H_2O$) 99.9 %, silver nitrate ($AgNO_3$) 99.9999 %, sodium acrylate (SA) 97 %, trisodium citrate (SC) 99.0 %, sodium chloride (NaCl) 99.0 %, calcium chloride ($CaCl_2$) 96.0 %, hydrochloric acid (HCl) 37 %, and common solvents were obtained from Aldrich. 3-amino-1,2,4-triazole-5-thiol (ATT) 98.0% was obtained from Tokyo Chemical Industry. Water was purified with a Millipore Direct-Q system (18.2 MΩ). 3-aminopropyltrimethoxysilane (APTMS) was obtained from Wako Pure Chemical Industries and was used to functionalize the surface of glass slides as a substrate for Raman analysis. Dialysis membranes with molecular weight pore size of 10,000 daltons were obtained from Spectra/Por and were rinsed in pure water before use.

2.2. Instrumentation and measurements

Techniques including transmission electron microscopy (TEM), Scanning TEM equipped with a High Angle Annular Dark Field detector (STEM-HAADF), Energy Dispersive Spectroscopy (EDS) elemental mapping, Raman spectroscopy and Ultraviolet-visible spectroscopy (UV-Vis) were used to characterize the size, shape, composition and other properties of the NPs. TEM analysis was performed on an Hitachi H-7100 instrument operated at 100 kV. STEM-HAADF and EDS elemental mapping were performed on a Jeol JEM-ARM200F operated at 200 kV with a sperical aberration corrector, the nominal resolution is 0.8 Å. Samples for TEM, STEM-HAADF and EDS elemental mapping were prepared by dropping the suspended NPs onto a carbon coated copper grid and drying in air overnight. Raman spectra were obtained with an Ar^+ laser (wavelength 514.5 nm, power 50 mW), using a Horiba-Jobin Yvon Ramanor T64000 triple monochromator equipped with a CCD

detector. The nonpolarized Raman scattering measurements were set under a microscope sample holder using a 180° backscattering geometry at room temperature. The laser spot diameter was 1 μm. An acquisition time of 10 seconds per spectrum was used with averaging of 3 spectra per analysis area.

2.3. Nanoparticle synthesis

2.3.1. Ag NP Synthesis. Ag NPs were synthesized by the acrylate reduction method [8]. Briefly, 50 ml of water was used to dissolve 1.25×10^{-5} moles of $AgNO_3$, and then 6.75×10^{-6} moles of NaOH were slowly added to the solution, which results in a dilute yellow-colored suspension of silver hydroxide [8]. This solution is purged with argon and is then brought to reflux. At reflux, 2.55×10^{-4} moles of SA are added, causing the suspension to turn completely clear. The solution is refluxed for 1 h, during which time the colour changes from clear to green-yellow and finally to amber-yellow. The as-synthesised Ag NPs were purified before use by the dialysis method.

2.3.2. Au NP Synthesis. For the synthesis of Au NPs, the general citrate reduction method was used [7,23]. An aqueous solution of $HAuCl_4{\cdot}3H_2O$ (50 ml, 1.25×10^{-5} moles $HAuCl_4{\cdot}3H_2O$) was vigorously stirred and heated to reflux at 100 °C. Then, an aqueous solution of SC (0.5 ml, 0.17 moles SC) was added to the reaction solution. Refluxing was continued for 1 hour. The light yellow Au solution turned immediately clear and after 5 minutes the colour changed to purple, slowly to dark purple and over time became a wine red coloured solution. After refluxing, the mixture was cooled to room temperature and used without further processing.

2.3.3. Au@Ag NP Synthesis. The as-synthesized citrate-capped Au NPs were used as core particles (seeds) in the preparation of Au@Ag core@shell NPs. The Au NP dispersion (20 ml) was brought to reflux with stirring, and then 5 ml of a 20 mM solution of $AgNO_3$ (1.0×10^{-4} moles) and 5 ml of a 13.5 mM solution of SC (6.75×10^{-5} moles) were simultaneously added dropwise. The reaction solution was refluxed for 20 minutes and then left to cool to room temperature. The as-synthesised NPs were purified before use by the dialysis method. As a major advantage of the seed-mediated synthesis, the Ag shell thickness of the resulting Au@Ag core@shell NPs can be finely controlled by varying the amount of $AgNO_3$ added to the reaction solution.

2.4. Experimental details to test the particle stability

The Ag and Au@Ag NP stability was tested by exposing the NPs to three different electrolytes. These particles were exposed to NaCl, $CaCl_2$ and HCl. The concentration of Ag and Au@Ag NPs was not the same (due to limitations in the synthesis methods), so the relative concentration ratio of Cl^- ion in the electrolytes to the NP concentration was kept uniform in the experiments (it is important to note that a sufficient amount of chloride is used in all cases to completely convert all Ag in the samples to AgCl). The as-synthesized Au NPs have a concentration of 1.2×10^{-8} M, while as-synthesized Ag NPs are 4.9×10^{-11} M, and Au@Ag NPs are 4.8×10^{-9} M. 1 ml of the Ag NPs was exposed to each of the three electrolytes including 10 µl of a 0.01 M solution of NaCl, 10 µl of a 0.005 M solution of $CaCl_2$ and 10 µl of a 0.01 M solution of HCl, resulting in a Cl^-/NP concentration ratio of 2.1×10^6 for each case. Similarly, 1 ml of the Au@Ag NPs was exposed to each of the three electrolytes including 10 µl of a 1 M solution of NaCl, 10 µl of a 0.5 M solution of $CaCl_2$ and 10 µl of a 1 M solution of HCl, resulting in a Cl^-/NP concentration ratio of 2.1×10^6 for each case. Finally, 1 ml of the Au@Ag NPs was also exposed to higher amounts of NaCl including both 25 and 100 µl of a 1 M solution. For all cases, the NPs were allowed to react with the added salt at ambient conditions (exposed to the atmosphere) for 24 hours to allow complete reaction between the Ag and the added Cl^- ions (and oxygen in the atmosphere). The extended reaction time was used to minimize kinetic reaction effects and allowed the particles to reach a final steady state in terms of particle structure/composition. After this time, the samples were gently centrifuged, rinsed with pure water and then were prepared for analysis. TEM sample drying effects were eliminated by allowing the NP samples an extended interaction time with the added electrolyte followed by centrifugation and sample washing. The resulting TEM samples showed uniform particle morphology and structures across the entire grid. It is also important to note that it was not feasible to collect UV-Vis measurements during the addition of the various electrolytes because the high electrolyte excess caused the SPR band to immediately be nearly completely suppressed.

2.5. NP TEM size assessment

NP size distributions as well as shell thicknesses were calculated by sizing particles from the corresponding TEM images. Multiple images were used in the particle size calculations for each sample and about 100 particles were

used to create each size distribution in order to obtain a statistical average.

3. Results and discussion

3.1. General morphology, structure and optical properties

The experimental results are discussed primarily in terms of the relative stability between Ag, and Au@Ag NPs. The relative stability of each NP sample was assessed by comparing the particle composition, morphology and structure both before and after exposing the particles to Cl-containing electrolytes. First, the morphology and optical properties of each as-synthesized particle sample were assessed. Figure 1 shows the UV-Vis spectrum and TEM image of each as-synthesized NP sample. In general, the colloidal dispersion of Ag NPs is a pale yellow coloured transparent solution with a LSPR band at 402 nm. The Ag NPs have a spherical morphology and a size of 15.2 ± 1.5 nm. The Au NPs are a deep-red colour with a LSPR band at 518 nm. The particles have a uniform and spherical morphology with a mean diameter of 14.2 ± 0.7 nm. These particles were used as seeds for the formation of Au@Ag NPs. Finally the Au@Ag NPs are a light red/pink colour with a primary LSPR band at 382 nm and a less intense shoulder band at approximately 490 nm. The particles retained the spherical morphology after coating with Ag as evidenced in the TEM image with a size of 20.4 ± 1.2 nm. The Ag shell thickness for these Au@Ag NPs is 3.1 nm, which corresponds very closely to the theoretical shell thickness (3.0 nm, calculated from the metallic feeding ratio). The real shell thickness was calculated by subtracting the mean diameter of the Au seed NPs from those of the core@shell NPs. One of the advantages to using Au NPs as seeds for the further growth of Ag on the particle surface is the ability to more closely control the final particle monodispersity and morphology. The resultant Au@Ag NPs showed a higher degree of monodispersity in terms of size and shape in comparision to the monometallic Ag NPs [14].

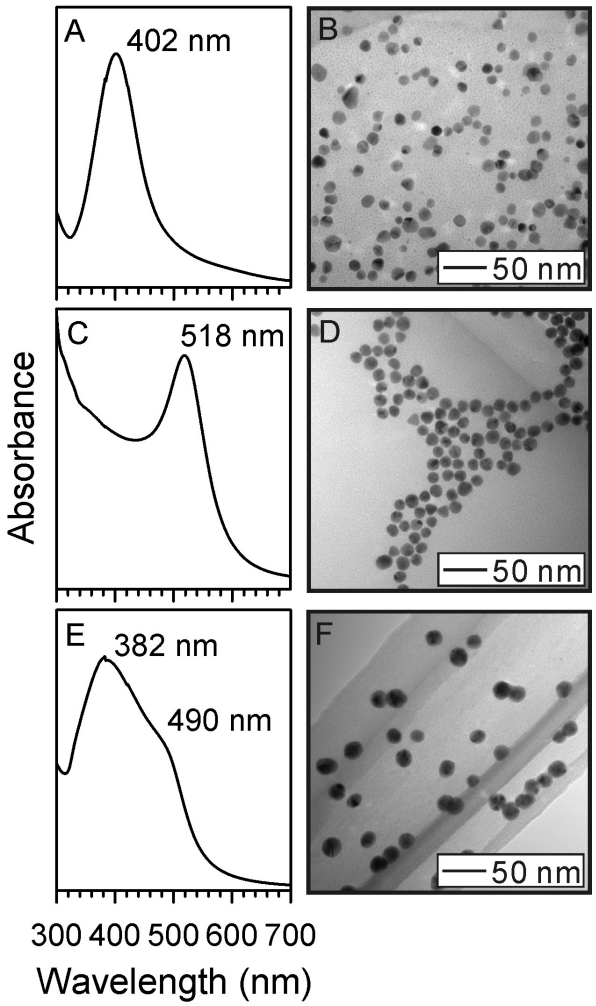

Figure 1. Representative UV-Vis spectra and TEM images for Ag (A, B), Au (C, D) and Au@Ag (E, F) as-synthesized NPs.

To provide definitive characterization of the core@shell nature of the Au@Ag NPs, STEM-HAADF imaging and EDS elemental mapping were performed. Figure 2 shows a STEM-HAADF image of a single Au@Ag NP as well as the corresponding two dimensional maps for Au and Ag in the particle. The high degree of atomic number (Z) based contrast offered by the STEM-HAADF technique allows the relative position of Au and Ag in the NP to be directly observed. The Au core is observed as the bright central region of the particle while the Ag appears as a lighter uniform halo around the brighter core. In addition, the EDS mapping result shows the relative locations of Au and Ag within the particle. Mapping of the Au M region is shown in green while the Ag L region is shown in red. By overlapping the two maps it is observed that the Au is located in the center of the particle area (the core) while the Ag is found on the outside (the shell). The collective EDS mapping and STEM-HAADF

results provide definitive evidence of the Au@Ag structure of the particles [14,15].

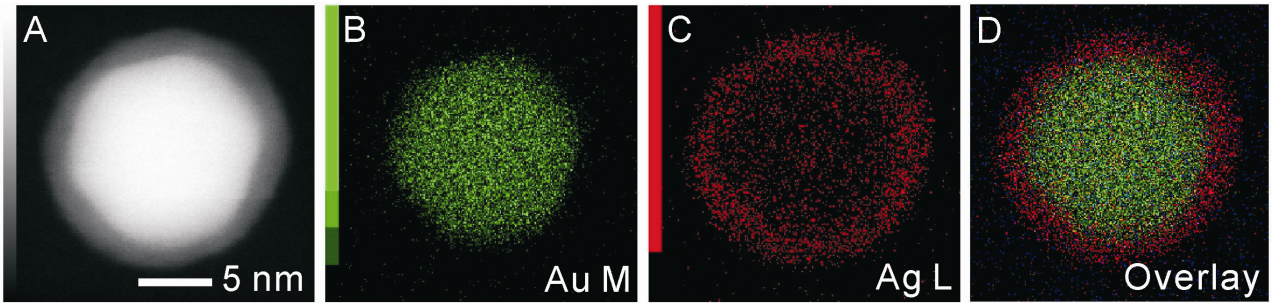

Figure 2. STEM-HAADF (A) and EDS elemental mapping images of a single Au@Ag NP for Au M map (B), Ag L map (C) and an overlay of the Au and Ag maps (D). The scale bar in (A) applies to all images.

3.2. Assessment of the particle stability

Next, the relative stability for the Ag and Au@Ag NP samples was tested by exposing the NPs to three different Cl-containing electrolytes including NaCl, $CaCl_2$ and HCl. Cl-containing electrolytes were chosen because of the well known oxidative etching phenomenon that exists when Ag metal is exposed to the ambient atmosphere and Cl^- ions, in addition to the fact that the detection of bio-molecules typically requires a buffer solution which contains significant amounts of Cl-containing electrolyte/salt such as NaCl, $CaCl_2$ and/or HCl. As a further parameter for the experiments, three fundamentally different electrolyte systems were chosen. A monovalent, divalent and an acidic electrolyte were used to test the fundamental effect on the NP stability with these electrolyte systems.

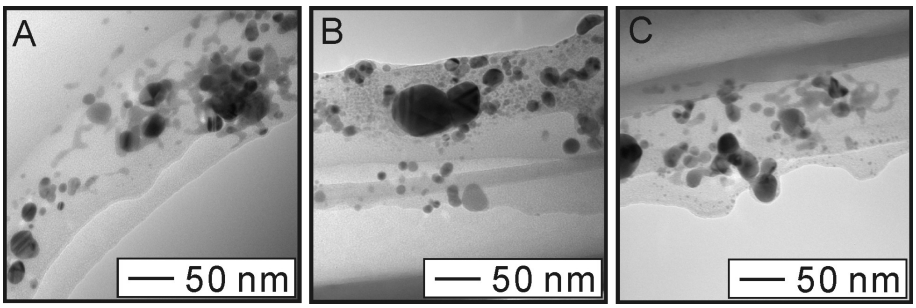

Figure 3. TEM images for Ag NPs exposed to NaCl (A), $CaCl_2$ (B) and HCl (C) after 24 hours when the Cl^-/NP concentration ratio is 2.1×10^6.

3.2.1. General stability of Ag NPs in the presence of Cl^- electrolytes. First the Ag NPs were exposed to the three

different types of electrolytes. Figure 3 shows the representative TEM images obtained after 24 hours for adding NaCl (figure 3A), $CaCl_2$ (figure 3B) and HCl (figure 3C). The Cl^-/NP concentration ratio is fixed at 2.1×10^6 for each sample to standardize the relative amount of Cl^- ions available to react with Ag in each system. It can be observed that each sample experienced the oxidative etching effect as evidenced by the appearance of large aggregates, larger particle sizes and overall a loss of particle dispersity. In these cases, the Ag has been completely oxidized and converted to AgCl through the oxidative etching process [3,21,24]. This oxidative etching phenomenon has previously been taken advantage of to selectively etch away small Ag seed particles of a specific geometry, leading to highly monodispersed Ag NPs with a highly uniform shape [1]. In general, the oxidative etching process consists of three steps. First, metallic Ag becomes oxidized in the presence of oxygen as illustrated in equation 1 [21,24]. Next, the silver oxide reaches an equilibrium state with the surrounding aqueous medium creating silver and hydroxide ions as shown in equation 2 [21,22]. Finally, the Cl^- ions in the system react with the Ag ions to form insoluble AgCl, shown in equation 3 [3.] In this way, as long as there is a sufficient supply of oxygen and Cl^- ions, a sample of Ag can be completely oxidatively etched away, leading to AgCl. For our Ag NP sample, this readily occurs in the presence of each Cl-containing electrolyte system, leading to complete destruction of the original Ag NPs, forming non-disperse AgCl.

$$2Ag^0 + \frac{1}{2}O_2 \rightarrow Ag_2O(s) \quad (1)$$

$$Ag_2O(s) + H_2O \leftrightarrow 2Ag^+ + 2OH^- \quad (2)$$

$$Ag^+ + Cl^- \rightarrow AgCl(s) \quad (3)$$

3.2.2. Stability of Au@Ag NPs in the presence of NaCl. Next, the stability of the Au@Ag NPs was first examined by exposing the NPs to the NaCl electrolyte system. Figure 4 shows the TEM images acquired for Au@Ag NPs exposed to three different concentrations of NaCl including Cl^-/NP concentration ratios of 2.1×10^6 (figure 4A), 5.3×10^6 (figure 4B) and 2.1×10^7 (figure 4C). In each case it can be observed that the NPs maintained a spherical morphology. The particles also appear to remain relatively well dispersed without severe aggregation. While the particle morphology remained spherical, the mean particle size decreased for each sample. For the Cl^-/NP

concentration ratio of 2.1×10^6, the NP size decreased to 18.8 ± 1.6 nm (a Ag shell thickness of 2.3 nm), the Cl^-/NP concentration ratio of 5.3×10^6 led to a size of 16.8 ± 1.7 nm (a Ag shell thickness of 1.3 nm) and finally the Cl^-/NP concentration ratio of 2.1×10^7 gave a particle size of 16.4 ± 1.5 nm (a Ag shell thickness of 1.1 nm). While a sufficient amount of chloride was used to completely convert all of the Ag in the samples to AgCl (an order of magnitude more Cl^- than Ag for a ratio of 2.1×10^6, two orders of magnitude excess Cl^- for a ratio of 2.1×10^7), a large amount of elemental Ag remains at the particle surface. The fact that the Ag shell thickness could not be reduced to less than 1 nm suggests that a critical Ag layer thickness exists where the electron transfer phenomenon inhibits all oxidative etching, despite the amount of Cl^- added. The particles also retained a high degree of monodispersity under every concentration of NaCl used, as evidenced by the size distributions. The retained NP stability in terms of resistance to aggregation has implications to bio-molecular sensing, especially in cases where high amounts of salt are required, for example in DNA detection where hybridization only occurs at salt levels of at least 0.05 M [5]. It is interesting to note that AgCl could not be found in the TEM analysis. It is likely that an insufficient amount of AgCl formed in these experiments to lead to a significant accumulation of the material in any one spot on the TEM grid.

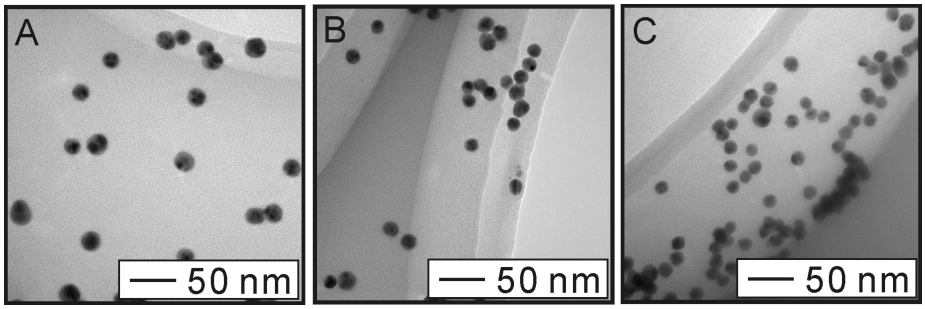

Figure 4. TEM images of Au@Ag NPs in NaCl after 24 hours when the Cl^-/NP concentration ratio is 2.1×10^6 (A), 5.3×10^6 (B) and 2.1×10^7 (C).

3.2.3. Assessment of the Au@Ag NP structure after NaCl exposure. To confirm that Ag metal remains at the Au@Ag particle surface STEM-HAADF and EDS elemental mapping were used to study the NPs exposed to the NaCl with an Cl^-/NP ratio of 2.1×10^6. Figure 5 shows the STEM-HAADF image and the elemental mapping results for Au and Ag. It can be observed in the STEM-HAADF image that the Au core still exists at the center of the particle after exposure to NaCl and more significantly that the Ag shell is still observed as the less bright halo

at the particle periphery. The elemental mapping shows that the Au is contained in the particle interior while the Ag remains at the particle surface. The results show that the Au@Ag NPs retain their structural and compositional integrity, even after exposure to relatively high levels of NaCl. In addition, the EDS analysis also confirmed that both chloride and oxygen do not exist in the mapped sample in significant amounts (beyond a monolayer of coverage, which is not observable in the elemental mapping image), which confirms that the remaining Ag in the particle shell is monometallic in nature without oxidation or conversion to AgCl.

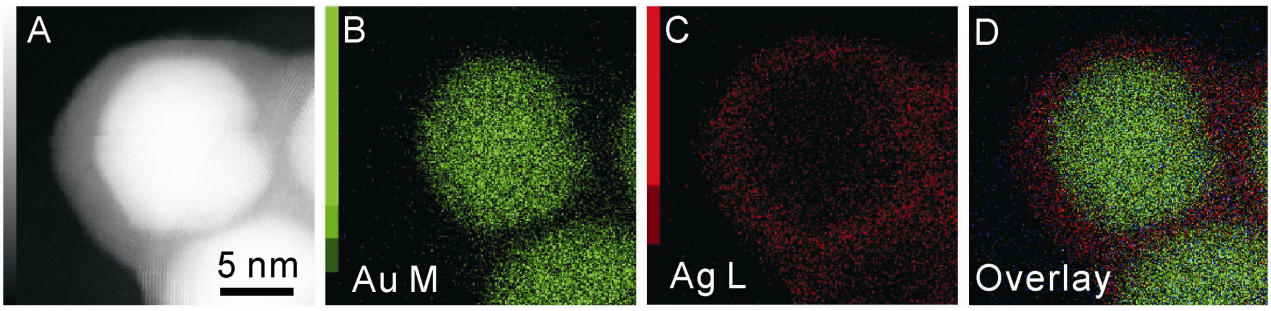

Figure 5. STEM-HAADF image (A), and EDS elemental mapping of Au@Ag NPs in NaCl after 24 h when the Cl^-/NP ratio is 2.1×10^6 for Au M map (B), Ag L map (C) and an overlay of the Au and Ag maps (D). The scale bar in (A) applies to all images.

3.2.4 Exposure of Au@Ag NPs to $CaCl_2$ and HCl. When the Au@Ag NPs are exposed to $CaCl_2$ or HCl, a slightly different phenomenon is observed. Figure 6 shows the representative TEM images collected for Au@Ag NPs exposed to $CaCl_2$ and HCl after 24 hours when the Cl^-/NP concentration ratio is 2.1×10^6. In the images the particles appear to be aggregated, oftentimes forming chainlike structures. Despite the fact that the particles appear to have undergone an aggregative process, the mean size of the particles was estimated to gauge whether or not Ag shell was lost to oxidative etching. It was found that for the case of $CaCl_2$ the particle size is approximately 16.1 ± 1.2 nm (a Ag shell thickness of 1.0 nm) while for HCl the particle size is about 15.6 ± 0.6 nm (a Ag shell thickness of 0.7 nm). Interestingly, the Ag shell could not be etched away completely in either of these two cases.

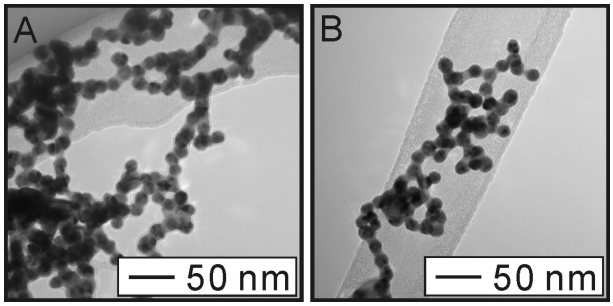

Figure 6. TEM images of Au@Ag NPs for $CaCl_2$ (A) and HCl (B) after 24 hours when the Cl^-/NP concentration ratio is 2.1×10^6.

3.2.5 *Assessment of the Au@Ag NP structure after $CaCl_2$ and HCl exposure.* In order to confirm whether or not the NPs retain any of the Ag shell, STEM-HAADF and EDS elemental mapping were used. Figure 7 shows the morphology, structure and composition results for the Au@Ag NPs exposed to $CaCl_2$. In the STEM-HAADF image, the Au particle cores retained their morphological integrity as evidenced by the observation of the brighter spheres in the image. Some Ag also remains as evidenced by the less bright material observed between the Au cores. The elemental mapping shows that the Au is still confined to the particle interior (the core) while the material between the particles is Ag. A small amount of Ag is also observed as a thin layer at the particle periphery exposed to the outside medium. In many cases, no clear boundary can be observed remaining in the Ag between particles. The images suggest that the individual particles have become fused together through the remaining Ag in the shell. Some small dim particles are also observed around the necklace-like structure in the STEM image, indicitave of the formation of small AgCl particles. Chloride and oxygen were not observed in the elemental mapping analysis.

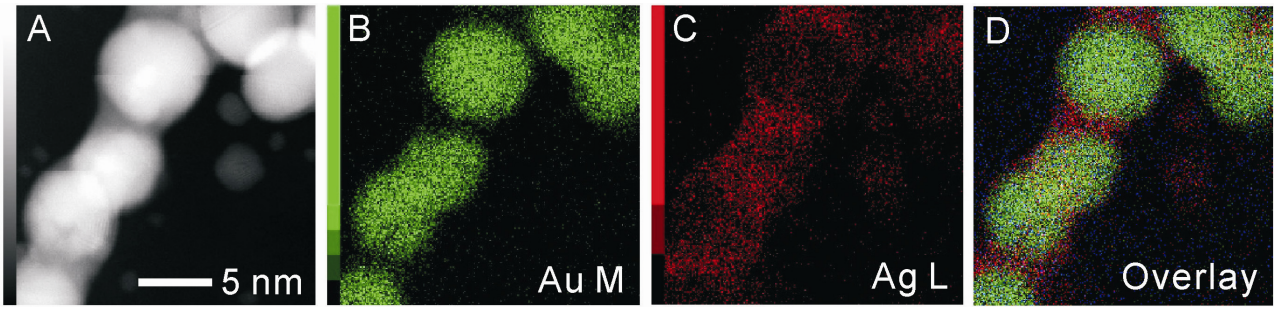

Figure 7. STEM-HAADF image (A), and EDS elemental mapping images of Au@Ag NPs for $CaCl_2$ after 24 hours when the Cl^-/NP concentration ratio is 2.1×10^6 for Au M map (B), Ag L map (C) and an overlay of the Au and Ag maps (D). The scale bar in (A) applies to all images.

For the case of exposing the Au@Ag NPs to HCl, the STEM-HAADF and EDS elemental mapping analysis reveal a similar structure/morphlogy to the $CaCl_2$ case. Figure 8 shows the STEM-HAADF and elemental mapping images taken for the Au@Ag NPs exposed to HCl. In the STEM-HAADF image a chain of NPs is observed with the Au cores appearing as the brighter spheres and the remaining Ag appearing as the less bright material between the Au cores. Some smaller particles can also be observed in the lower half of the STEM image indicating that some AgCl particles formed through the oxidative etching process. The elemental mapping images confirm that the Au remains in the particle center (the core) while the material between the particles is Ag, with a thin layer of Ag remaining on the outside of the particles exposed to the outside medium. These particles also appear to have fused as evidenced by the lack in a clear boundary in the silver between particles. Chlorine was not observed, but a faint blue colour can be observed in the overlay image (figure 8D) in the area surrounding the NP chain which indicates the presence of a faint amount of oxygen (mapping of the oxygen K line).

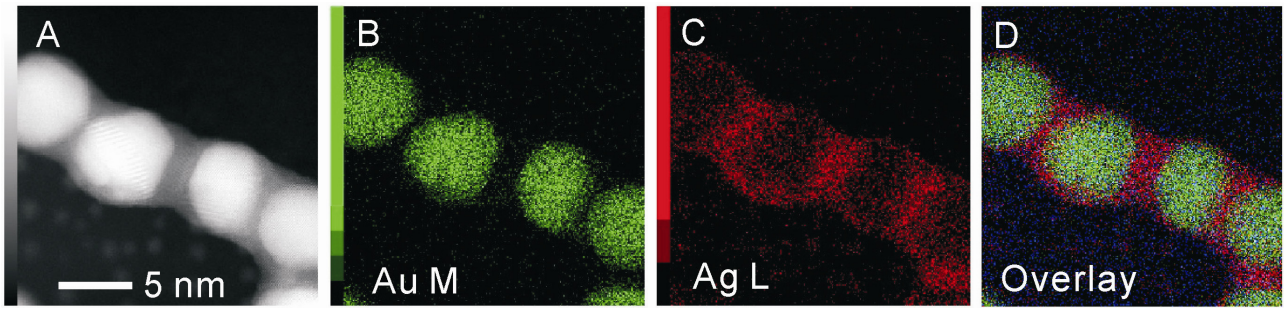

Figure 8. STEM-HAADF image (A), and EDS elemental mapping images of Au@Ag NPs for HCl after 24 hours when the Cl^-/NP concentration ratio is 2.1×10^6 for Au M map (B), Ag L map (C) and an overlay of the Au and Ag maps (D). The scale bar in (A) applies to all images.

When the Au@Ag NPs are exposed to $CaCl_2$ or HCl a similar phenomenon occurs as evidenced by the similar structure, composition and morphology of the resulting materials. However, the phenomenon is quite different from the case of Au@Ag NPs exposed to NaCl. This clearly indicates that the cations in electrolytes also play a significant role in the aggregation and etching processes. Once the particle sample is exposed to either of these two electrolytes, two primary competing effects take place. First, the particles begin to be oxidatively etched by the presence of ambient oxygen and the Cl^- ions. At the same time the particles also undergo aggregation as a result of screening of the negative surface charge of the NPs by cations in the electrolyte added. The observed morphology and structure of the resulting aggregates suggests that it is the aggregation step that dominates the

process, occuring quickly, causing the particles to aggregate and form the necklace-like structures, which is followed by a slower oxidative etching process, removing some Ag from the exposed surfaces of the particles. This explains why relatively more Ag is observed as the material fusing the Au cores together in the aggregates, while less is observed exposed to the outside medium in the STEM-HAADF and EDS elemental mapping images. The observation of the neclace like structures is intriguing and cannot be explained based solely on the above aggregative processes. It is likely that other factors such as the relative concentration of NPs and electrolytes contribute to the formation of the necklace strand aggregates.

For the case of NaCl, the Au@Ag NPs appear to resist the aggregation step (a small degree of aggregation is observed as the amount of added NaCl increases), so only the oxidative etching takes place. In the case of $CaCl_2$, the Ca^{2+} in the electrolyte reacts with the ambient citrate molecules (used for particle capping and stabilization) causing insoluble calcium citrate to form. This causes an additional disturbance in the adsorption of the citrate capping agent on the particle surface, effectively de-protecting the Au@Ag NPs and leading to accelerated NP aggregation. For the case of HCl, when the NPs are exposed to this acid, the pH of the solution also changes. The pH approaches a value of 2, leading to removal of citrate from the particle surface (citrate has three negatively charged carboxyl groups with $pk_{a1} = 3.1$, $pk_{a2} = 4.8$ and $pk_{a3} = 6.4$) [7], also causing de-protection of the NPs and accelerated aggregation. In this case, the etching rate is also significantly affected as evidenced by the final Ag shell thickness of 0.7 nm (the thinnest for all cases). This occurs because the second step in the oxidative etching process (equation 2) is pH dependent and is accelerated at low pH.

3.3. Assessment of the sensing properties

To test and compare the effectiveness of the Ag and Au@Ag NPs as sensing probes, an experiment was performed where Ag and Au@Ag NPs (1 mL of each) were exposed to NaCl (a Cl^-/NP concentration ratio of 2.1×10^7) and ATT (0.005 mM total ATT concentration, a large excess in terms of completely coating the surfaces of the NPs). The ATT is expected to adsorb to the NP surfaces via the thiol moity and act as a Raman active reporter molecule [25]. The presence of the NaCl mimics the ambient level of salt needed for detection of biomolecules, and also assists in aggregation and precipitation of the NPs through electrostatic screening of the repulsive charges. After 24 hours of exposure, the precipitated NPs were gently rinsed with pure water to remove

excess reactants, and then were dropped onto an APTMS coated glass substrate. The samples were dried in ambient conditions and were analyzed using Raman spectroscopy. Five different sample areas were inspected for both Ag and Au@Ag NP samples. Figure 9 shows the resulting Raman spectra collected for each sample. For the Ag NPs, a single broad peak with varying intensity is observed centered at about 1345 cm^{-1} while for the Au@Ag NPs, three distint peaks with relatively uniform intensity are observed at about 1270, 1355 and 1420 cm^{-1}. The Raman spectra collected for the Au@Ag NPs is characteristic for ATT laying flat on a metal surface through bidentate bonding arising from the triazole ring vibrations [26,27]. While the weak and broad peak observed for the Ag NP case could be attributed to a weak band for ATT having a more perpendicular orientation to the metal surface [26,27], enhancement by the presence of Ag_2O [28] or chemical enhancement by the presence of Cl^- [29] the fact that no other characteristic bands are observed in the spectrum, even at a shifted position, is a strong indication that the interaction between ATT and the Ag NP sample is relatively weak. This can be explained by the sample preparation technqiue in which the ATT should adsorb to the NP surface, then be precipitated along with the particles to be cast on the APTMS coated glass substrate. However, as shown in the case for exposing the Ag NPs to a high level of NaCl, all of the particles are completely converted to insoluble AgCl. In this case, the ATT does not have a strong interaction with the AgCl, resulting in weak adsorbtion to the surfaces of particles. The excess ATT was likely removed in the rinsing step of the sample preparation. As a result, the band observed at about 1345 cm^{-1} for the Ag NPs probably originates from the ATT molecules weakly adsorbed onto AgCl surfaces having a perpendicular orientation. Despite this, if we assume that the bands observed at 1345 and 1355 cm^{-1} for Ag and Au@Ag NPs are characteristic for ATT, the standard deviation associated with the intensity at the maxima of the peaks in each sample can be assessed. For the Ag NP case the average intensity was found to be 93 ± 38 counts/sec while for the Au@Ag NPs the intensity is 207 ± 20 counts/sec. The Ag NPs show an intensity deviation of about 41% while the Au@Ag NPs have a deviation of only 10%. The experimental results show that the Au@Ag NPs display a reliable and reproducible sensing capability in the presence of salt and demonstrates the feasibility of using these materials in applications such as biomolecular detection that demand the presence of a high amount of electrolytes such as NaCl. It should be noted that in this experiment, the NP characteristics such as size, shape, composition or thickness of the Ag shell were not optimized for the detection. In addition, a thin layer of Ag_2O may exist at the surface of the Au@Ag NPs in this experiment, which would

dampen the enhanced Raman signal obtained [28]. Despite this, the results illustrate the robustness of the Au@Ag NPs and demonstrates the practicality of using these probes for the detection of biomolecules in environments with high levels of salt.

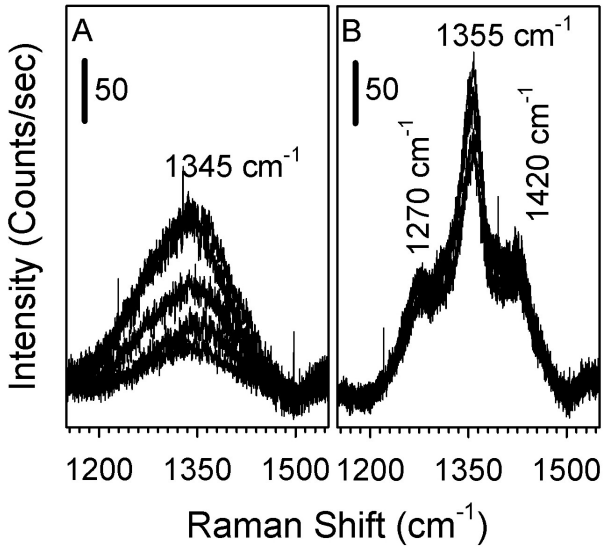

Figure 9. Raman spectra taken for Ag NPs (A) and Au@Ag NPs (B) exposed to ATT and NaCl with a Cl^-/NP concentration ratio of 2.1×10^7.

In general, the Au@Ag NPs showed enhanced stability when exposed to each of the different types of Cl-containing electrolytes, mainly because the first step in the oxidative etching process (equation 1) is suppressed due to the electron transfer from the Au core to the Ag shell leading to a negative oxidation state of Ag. For the case of NaCl, the NPs resisted both aggregation and oxidative etching, even at high concentrations of electrolyte. In the cases of $CaCl_2$ and HCl the particles displayed limited aggregation due to the de-protection of Au@Ag NP surfaces owing to the different effects of cations, but still resisted oxidative etching of the Ag shell. It is important to note that in all cases the Ag shell thickness was reduced after exposure to the different electrolytes, but a crital shell thickness of ~1 nm exists where further etching appears to be suppressed, supporting the fact that the electron transfer effect is an interfacial phenomenon. Raman analysis of each NP sample exposed to NaCl and ATT shows a reliable and reproducible signal in the case of using Au@Ag NPs, demonstrating the feasibility of using these probes for practical biomolecular sensing.

4. Conclusions

When Ag NPs are exposed to Cl-containing electrolytes they undergo the oxidative etching phenomenon, leading to the formation of AgCl. This phenomenon makes monometallic Ag NPs non-ideal for sensing and bio-diagnostics applications. When Au core particles were coated in Ag, an electron transfer phenomenon occurs that imparts increased stability against the oxidative etching phenomonen. This was evidenced by the increased stability of the Ag shell component in Au@Ag NPs exposed to three different Cl-containing electrolytes including NaCl, $CaCl_2$ and HCl. When the Au@Ag NPs were exposed to NaCl, the particles resisted aggregation and complete oxidative etching, while for $CaCl_2$ and HCl, limited aggregation took place and the oxidative etching effect was suppressed. The results illustrate that Au@Ag NPs display unique electronic properties that can be manipulated to create NP probes for sensing and diagnostics that display unprecedented stability against oxidation. Such an ability can lead to the development of a new generation of highly active and stable NP probes.

5. Acknowledgements

We thank Dr. M. Koyano for his assistance with Raman measurements.

6. References

[1] Wiley B, Sun Y, and Xia Y 2007 *Acc. Chem. Res.* **40** 1067

Wiley B, Sun Y and Xia Y 2005 *Langmuir* **21** 8077

[2] Lu L, Kobayashi A, Tawa K and Ozaki Y 2006 *Chem. Mater.* **18** 4894

[3] Shon Y S and Cutler E 2004 *Langmuir* **20** 6626

[4] Pillai Z S and Kamat P V 2004 *J. Phys. Chem.* B **108** 945

[5] Cao Y W, Jin R and Mirkin C A 2001 *J. Am. Chem. Soc.* **123** 7961

Rosi N L and Mirkin C A 2005 *Chem. Rev.* **105** 1547

Mirkin C A, Letsinger R L, Mucic R C and Storhoff J J 1996 *Nature* **382** 607

Taton T A, Mirkin C A and Letsinger R L 2000 *Science* **289** 1757

[6] Cui Y, Ren B, Yao J L, Gu R A and Tian Z Q 2006 *J. Phys. Chem.* B **110** 4002

[7] Lim I-I S, Ip W, Crew E, Njoki P N, Mott D and Zhong C J 2007 *Langmuir* **23** 826

Lim I-I S, Mott D, Ip W, Njoki P N, Pan Y, Zhou S and Zhong C J 2008 *Langmuir* **24** 8857

Lim I-I S, Mott D, Engelhard M H, Pan Y, Kamodia S, Luo J, Njoki P N, Zhou S, Wang L and Zhong C J

Anal. Chem. **2009**, *81*, 689.

Lim I-I S, Goroleski F, Mott D, Kariuki N N, Ip W, Luo J and Zhong C J 2006 *J. Phys. Chem.* B **110** 6673

[8] Mott D, Thuy N T B, Aoki Y and Maenosono S 2010 *Phil. Trans. R. Soc.* A **368** 4275

[9] Njoki P N, Lim I-I S, Mott D, Park H Y, Khan B, Mishra S, Sujakumar R, Luo J and Zhong C J 2007 *J. Phys. Chem.* C **111** 14664

[10] Thuy N T B, Yokogawa R, Yoshimura Y, Fujimoto K, Koyano M and Maenosono S 2010 *Analyst* **135** 595

[11] Ma Y, Li W, Cho E C, Li Z, Yu T, Zeng J, Xie Z and Xia Y 2010 *ACS Nano* **6** 6725

Sun Y and Xia Y 2002 *Anal. Chem.* **74** 5297

Sun Y and Xia Y 2004 *Am. Chem. Soc.* **126** 3892

[12] Rodríguez-González B, Burrows A, Watanabe M, Kiely C J and Marzán L M L 2005 *J. Mater. Chem.* **15** 1755

Pande S, Ghosh S K, Praharaj S, Panigrahi S, Basu S, Jana S, Pal A, Tsukuda T and Pal T 2007 *J. Phys. Chem.* C **111** 10806

[13] Tyson C C, Bzowski A, Kristof P, Kuhn M, Sammynaiken R and Sham T K 1992 *Phys. Rev.* B **45** 8924

[14] Anh D T N, Singh P, Shankar C, Mott D and Maenosono S *Appl. Phys. Lett.* **99** 073107

[15] Nishimura S, Anh T N D, Mott D M, Ebitani K and Maenosono S 2012 *J. Phys. Chem.* C **116** 4511

[16] Yang Y, Gong X, Zeng H, Zhang L, Zhang X, Zou C and Huang S 2010 *J. Phys. Chem.* C **114** 256

[17] Freeman R G, Hommer M B, Grabar K C, Jackson M A and Natan M J 1996 *J. Phys. Chem.* **100** 718

[18] Tsuji M, Miyamae N. Lim S, Kimura K, Zhang Xu, Hikino S and Nishio M *Cryst. Growth Des.* **6** 1801

[19] Selvakannan P R, Swami A, Srisathiyanarayanan D, Shirude P S, Pasricha R, Mandale A B and Sastry M 2004 *Langmuir* **20** 7825

[20] Polsky R, Gill R, Kaganovsky L and Willner I 2006 *Anal. Chem.* **78** 2268

Lee S, Cha E J, Park K, Lee S Y, Hong J K, Sun I C, Kim S Y, Choi K, Kwon I C, Kim K and Ahn C H 2008 *Angew. Chem.* **120** 2846

[21] Mulvaney P, Linnert T and Henglein A 1991 *J. Phys. Chem.* **95** 7843

Henglein A 1998 *Chem. Mater.* **10** 444

Henglein A, Linnert T and Mulvaney P 1990 *Ber. Bunsen-Ges. Phys. Chem.* **94** 1449

[22] Kapoor S 1998 *Langmuir* **14** 1021

[23] Grabar K C, Freeman R G, Hommer M B and Natan M J 1995 *Anal. Chem.* **67** 735

[24] Yin Y D, Li Z Y, Zhong Z Y, Gates B, Xia Y N and Venkateswaran S 2002 *J. Mater. Chem.* **12** 522

Blaser S A, Scheringer M, MacLeod M and Hungerbühler K 2008 *Sci. Total Environ.* **390** 396

Chen M, Wang L Y, Han J T, Zhang J Y, Li Z Y and Qian D J 2006 *J. Phys. Chem.* B **110** 11224

Kumar R and Münstedt H 2005 *Biomaterials* **26** 2081

[25] Singh P, Thuy N T B, Aoki Y, Mott D and Maenosono S 2011 *J. Appl. Phys.* **109** 094301

[26] Wrzosek B and Bukowska J 2007 *J. Phys. Chem.* C **111** 17397

[27] Kudelski A 2010 *J. Phys. Chem.* B **114** 5180

[28] Han Y, Lupitskyy R, Chou T M, Stafford C M, Du H and Sukhishvili S 2011 *Anal. Chem.* **83** 5873

[29] Doering W E and Nie S 2002 *J. Phys. Chem.* B **106** 311